Recent Development in Chalcogenides for Supercapacitor Applications

G. M. Lohar, O. C. Pore, R. K. Kamble, and A. V. Fulari

Abstract The electrochemical supercapacitor, due to their rapid charge-discharge rates, good cyclic stability, high energy density, and power density are considered an ideal candidate for energy storage devices. For the high efficiency, improvement in performance, and electrochemical properties of supercapacitors; different nanostructured electrode materials have been studied. The efforts have been carried out to develop state-of-the-art high capacitive electrode materials for supercapacitors which enable high specific capacitance using rapid Faradaic redox reactions and provide ultra-high cyclic stability. Recent progress studies demonstrated that the transition metal chalcogenides especially NiX (X = S, Se, Te) are noteworthy candidates for highly efficient supercapacitor application because of their promising properties such as thermal stability, mechanical stability, superior intrinsic conductivity as compared to transition metal oxides and good cyclability. In the present chapter, we discussed the NiX (X = S, Se, Te) based materials for electrochemical supercapacitor application. Furthermore, we have summarized the supercapacitor performance of NiX (X = S, Se, Te) based nanomaterials. Lastly, the benefits and challenges of NiX (X = S, Se, Te) based materials for upcoming energy storage are discussed.

Keywords Metal chalcogenides · Supercapacitor · Specific capacitance

G. M. Lohar (✉) · O. C. Pore · R. K. Kamble
Department of Physics, Lal Bahadur Shastri College of Arts, Science and Commerce, Satara, M.S 415002, India
e-mail: gauravlohar24@gmail.com

O. C. Pore · R. K. Kamble
Holography and Materials Research Laboratory, Department of Physics, Shivaji University, Kolhapur, M.S. 416004, India

A. V. Fulari
Division of Physics and Semiconductor Science, Dongguk University, Seoul 04620, Republic of Korea

S. Thomas et al. (eds.), *Nanostructured Materials for Supercapacitors*,
Advances in Material Research and Technology,
https://doi.org/10.1007/978-3-030-99302-3_16

1 Introduction

The rapidly growing energy demand, energy consumption, and its consequences such as depletion of fossil fuels, pollution, and global warming, etc. attract the use of highly efficient, clean, energy consumption technologies and renewable energy resources. In recent years, different energy storage devices for example conventional capacitors, fuel cells, batteries, and supercapacitors receiving more attention from researchers. Among these devices, supercapacitors with their promising properties such as low maintenance costs, fast charging-discharging rate, high power density, high cyclic stability, and safe operation play a crucial role in electrochemical energy storage devices [1–3]. Based on charge storage mechanism, supercapacitors are of two types viz electric double-layer capacitors (EDLCs) and pseudocapacitors. The EDLCs store charges electrostatically at the electrode and electrolyte interface. Carbon-based materials are the EDLC type supercapacitors and they are suitable in the field of electronic equipment. But their relatively lower energy density restricts its application where high energy storage capability is required. In pseudocapacitors, reversible redox reactions are responsible for the charging-discharging process [4–6].

Different Metal oxides (MnO_2, Co_3O_4, Fe_2O_3, RuO_2, NiO, CuO), metal chalcogenides (NiS, MoS_2, VS_2, NiSe, NiTe, Cu_2S, CoS_2, and $NiCo_2S_4$), metal nitrides (RuN, VN, TiN, MoN), and conducting polymers have been utilized as pseudocapacitive electrode materials [4, 7]. The metal chalcogenides exhibit a better electrochemical supercapacitor performance as compared to metal oxides and replacing oxygen with chalcogenides is responsible for more flexibility for material organization. Out of these many materials transition metal chalcogenides; especially Sulphides, Selenides, and Tellurides have received more research interests as potential applications in supercapacitors. The better electrochemical supercapacitor performance of these transition metal chalcogenides is because of their unique crystal structures, tunable stoichiometric compositions, and redox-rich sites. Also, its higher electrical conductivity in comparison to respective transition metal oxide makes them a suitable candidate for supercapacitor application as compared to transition metal oxides [3, 8, 9].

Recently, the transition metals such as Ni, Co, Mn, Ti, and Fe and their compounds (oxides, hydroxides, and sulfides) have been extensively studied for electrochemical supercapacitor application. Among these transition metal base compounds, transition metal sulfides especially nickel sulfides resemble suitable candidates for supercapacitor application because of the slight difference in electronegativity of Ni ($\nu =$ 1.91 eV) and S ($\nu = 2.58$ eV), high specific capacitance value, high redox activity, high electrical conductivity, easy as well as low-cost preparation [10–12]. Selenium (Se) is the nearest element of sulfur (S) in the VI A group of the periodic table and exhibits the same oxidation states and valance electrons as sulfur. Hence, the electrochemical activities of metal selenides and metal sulfides almost resemble. The lower electronegativity of Te ($\nu = 2.1$ eV) as compared to S and Se ($\nu = 2.55$ eV) also attracting attention of researchers for their use in Ni-based metal chalcogenides [3, 13–15]. In the present chapter the NiX (X = S, Se, Te) based electrode materials,

their characterizations (XRD, FT-IR, Raman, XPS spectra), and their use in supercapacitor application are discussed. NiX (X = S, Se, Te) based electrode materials have been unveiled as cheap, promising, and eco-friendly materials for the development of supercapacitors.

2 Characterizations of NiX (X = S, Se, Te) Based Materials

Some characterizations such as X-ray diffraction (XRD), Fourier transform infrared spectroscopy (FT-IR), Fourier transforms Raman spectroscopy (FT-Raman), and X-ray photoelectron spectroscopy (XPS) of NiX (X = S, Se, Te) based materials for electrochemical supercapacitor application are mentioned. Parveen et al. [16] synthesized flower-like NiS nanostructures by solvothermal method. The XRD pattern (Fig. 1a) of as optimized NiS_10h electrode shows the characteristic peaks at 30.15°, 34.63°, 45.86°, 53.55°, 60.8°, 62.68°, 65.31°, 70.64°, and 73.13° which are corresponding to the planes (100), (101), (102), (110), (103), (200), (201), (004), and (202) respectively. These all peaks are related to JCPDS card number 10-075-0613 of NiS. Wu et al. [17] synthesized $Ni_{0.85}Se$ nanoparticles by tuning morphologies by using different solvents by simple solvothermal method. Figure 1b shows the XRD spectra of $Ni_{0.85}Se$ different NiSe nanostructures synthesized by using different solvents. The peaks at 33.3°, 45.0°, 50.7°, 60.3°, 62.5°, and 70.5° are assigned to planes (101), (102), (110), (103), (201), and (202) of $Ni_{0.85}Se$ JCPDS card number 18-0888. These results indicated the formation of high crystallinity and purity of $Ni_{0.85}Se$ nanostructures. Zhou et al. [18] developed NiTe directly deposited on NF for supercapacitor application for the first time. Figure 1c depicts the XRD spectrum of the NiTe electrode. The peaks at 58.61°, 46.52°, 43.41°, 31.54°, and in the XRD pattern of NiTe are correspond to the crystalline plane (103), (110), (102), (101) and respectively. These peaks are corresponding to the JCPDS card number 38–1393 corresponding to the hexagonal crystalline structure of NiTe. Karthikeyan et al. [19] synthesized NiS nanoparticles with a precursor hot-injection method. The FT-IR study reveals that the peaks at 2921/2852, 3400, and 1653 cm^{-1} are related to the C-H stretching, N-H stretching, and rocking vibrations respectively. Li et al. [20] prepared a composite of graphene and NiS_2 (graphene/NiS_2) by using a simple solvothermal reaction.

Figure 1d presents the FT-Raman spectrum of as-synthesized graphene/NiS_2 composite. The peak at 1580 and 1349 cm^{-1} corresponds to the G and D band of rGO respectively. Song et al. [21] developed Nickel selenide nanoparticles on carbon nanowires ($NiSe_2$/C NWs) by simple hydrothermal method and salinization strategy. Figure 1e shows the Raman spectra of $NiSe_2$/C electrode. The Raman shift in Fig. 1e at 1576 and 1349 cm^{-1} present the G and D band of carbon respectively. Inset of Fig. 1e shows the Raman spectra with an enlarged scale of $NiSe_2$/C NWs showing the peaks at 151.86, 169.24, 209.20, and 231.75 cm^{-1}. Kim et al. [22] prepared Ni_3S_2/Ni electrode with the help of a two-step electrodeposition method for supercapacitor application. Figure 1f and g presents the Ni 2p and S 2p spectrum of Ni_3S_2/Ni electrode. The two peaks in Ni 2p spectrum at 855.4 eV and 873.2 eV are

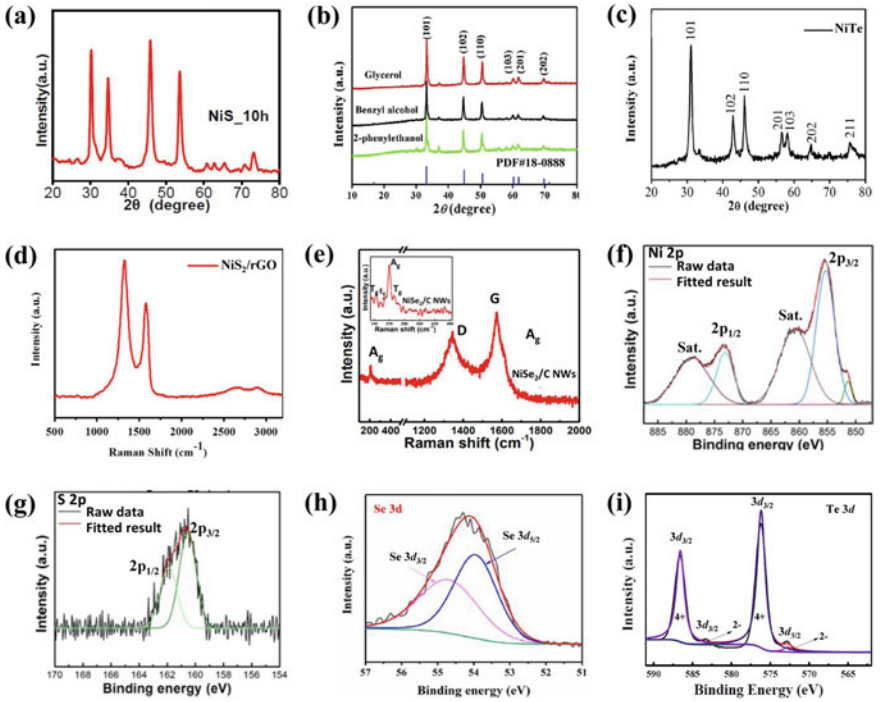

Fig. 1 **a** XRD pattern of NiS. Adapted with permission from [16], Copyright (2018), Elsevier. **b** XRD spectra of $Ni_{0.85}Se$ synthesized by using different solvents. Adapted with permission from [17], Copyright (2019), Elsevier. **c** XRD spectrum of NiTe. Adapted with permission from [18], Copyright (2016), Elsevier. **d** Raman spectrum of NiS_2/rGO. Adapted with permission from [20], Copyright (2015), Elsevier. **e** Raman spectrum of $NiSe_2$/C NWs (Inset: enlarged view of Raman spectra). Adapted with permission from [21], Copyright (2017), Elsevier. **f** the Ni 2p spectrum of Ni_3S_2/Ni 6 min electrode. Adapted with permission from [22], Copyright (2018), American Chemical Society. **g** and S 2p spectrum. Adapted with permission from [22], Copyright (2018), American Chemical Society. **h** XPS spectra of Se. Adapted with permission from [23], Copyright (2020), Elsevier. **i** XPS spectra of Te 3d spectrum. Adapted with permission from [24], Copyright (2019), Elsevier

related to Ni $2p_{3/2}$ and Ni $2p_{1/2}$ respectively. The peaks at 162.1 eV and 160.5 eV in S 2p spectra confirm the presence of Ni_3S_2. Zhao et al. [23] developed hierarchical Ni_3Se_2 nanodendrite arrays by a solvothermal method by a binder-free approach. Figure 1h shows the Se 3d spectrum of as-synthesized Ni_3Se_2. The peaks in Se 3d spectrum at 53.95 and 54.69 eV are related to Se $3d_{5/2}$ and Se $3d_{3/2}$ respectively which confirms the existence of Se^{2-}. Ye et al. [24] prepared cobalt-doped NiTe electrode (NiTe: Co) via the single-step hydrothermal method for electrochemical supercapacitor application. Figure 1i presents Te 4d spectrum. The characteristic bands at 583.3 eV as well as 572.8 eV are related to the Te^{2-}, while the peaks at 586.6 eV and 576.2 eV are related to Te^{4+}.

3 Recent Development in NiX (X = S, Se, Te) Based Electrode Materials for Supercapacitor Application

3.1 Nickle Sulfides

Zhang et al. [25] developed different β-NiS morphologies by two-step solvothermal method by varying volume ratios of a solvent such as ethanol, deionized water, and glycol. Out of different morphologies, flowerlike β-NiS electrode achieved 2425.89 F g^{-1} specific capacitance at 1 A g^{-1}. The better supercapacitor results of β-NiS flower-like electrode as compared to other morphologies (coral-like, urchin-like, and flake-like) raised due to its special pore structures and enlarge surface area as compared to other morphologies. These observations confirm that the flower-like β-NiS electrode performs a crucial role in achieving better specific capacitance. The as-synthesized β-NiS//Activated Carbon (β-NiS//AC) electrode achieved a maximum specific capacitance of 32.90 F g^{-1}. Kim et al. [22] developed Ni_3S_2/Ni electrodes with a two-step electrodeposition process. Figure 2a presents the synthesis process of Ni_3S_2/Ni electrode by electrodeposition method. The optimized Ni_3S_2/Ni electrode shows flaky morphology. The prepared electrode exhibited 786.5 C g^{-1} specific capacitance at 10 mA cm^{-2} as well as good capacity retention of 88.6% over 1000 cycles. Also, they have prepared (Asymmetric supercapacitor device) ASC device (Ni_3S_2/Ni 6 min//AC) which achieved a specific capacitance of 103.2 F g^{-1} at 1 A g^{-1} and cyclic stability of 93.9% after 6000 cycles. Darsara et al. [26] developed Ni_3S_4–NiS and Ni_3S_4–NiS@rGO hybrid by one-step hydrothermal method. SEM study of Ni_3S_4–NiS reveal the formation of starfish-like morphology with various dimensions (Fig. 2b). In the case of Ni_3S_4–NiS@rGO hybrid, starfish-like morphology of Ni_3S_4–NiS observed to be anchored on graphene surface plate. The Ni_3S_4–NiS and Ni_3S_4–NiS@rGO samples showed a BET surface area of 220 and 270 m^2 g^{-1} respectively. The prepared Ni_3S_4–NiS and Ni_3S_4–NiS@rGO electrodes achieved 1005 and 1578 F g^{-1} specific capacitance at 0.5 A g^{-1}.

The Ni_3S_4–NiS@rGO electrode exhibited 9% more stability as compared to Ni_3S_4–NiS electrode. The Ni_3S_4–NiS@rGO electrode exhibited more specific capacitance and stability as compared to Ni_3S_4–NiS electrode because the rGO in Ni_3S_4–NiS@rGO provides more surface area for electrolyte interaction and higher conductivity. Guan et al. [27] synthesized NiS-MoS_2 on carbon cloth having morphology hetero-nanosheet arrays (HNSAs) as shown in (Fig. 2c). The maximum specific capacity calculated for NiS-MoS_2 HNSAs//CC electrode was 271.7 mAh g^{-1} at 2.5 mA cm^{-2}. Also, it showed better cyclic stability of 78% over 3000 GCD cycles. Xu et al. [28] developed carbon nanofibers (CNFs) wrapped with NiS nanoparticles via electrospinning, calcination, and in situ sulfurization method. As shown in Fig. 2d CNFs-NiS show a netlike structure. This netlike structure is observed to be made up of many pores spread on a rough surface. It exhibited the highest 177.1 mAh g^{-1} specific capacity at 1 A g^{-1} with 88.7% cyclic stability after 5000 cycles.

Tan et al. [29] developed cabbage-like α-NiS using facile solvothermal method then annealing treatment. The CVs of α-NiS electrode at 5 to 50 mV s^{-1} scan rates are

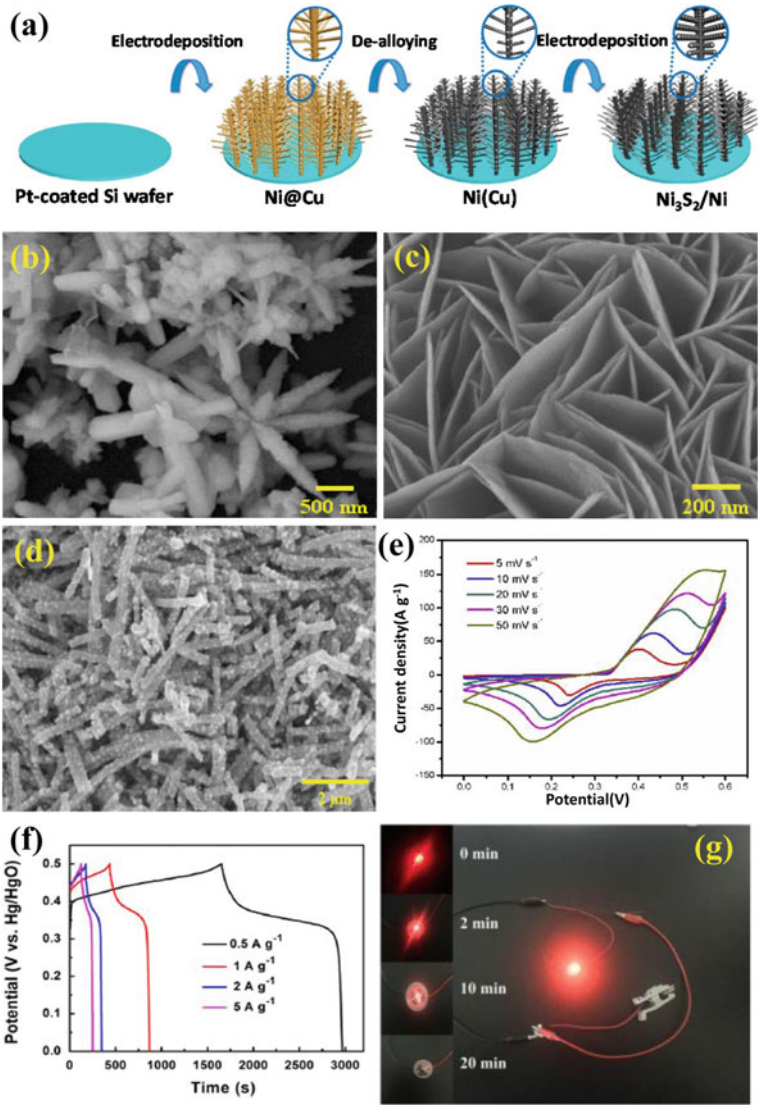

Fig. 2 **a** Schematic presentation of preparation of Ni_3S_2/Ni electrode. Adapted with permission from [22], Copyright (2018), American Chemical Society. **b** SEM image of Ni_3S_4–NiS. Adapted with permission from [26], Copyright (2021), Elsevier. **c** SEM image of NiS-MoS_2. Adapted with permission from [27], Copyright (2019), American Chemical Society. **d** SEM image of CNFs-NiS. Adapted with permission from [28], Copyright (2018), Elsevier. **e** CV curves of α-NiS electrode at various scan rates (5–50 mV s^{-1}). Adapted with permission from [29], Copyright (2019), Elsevier. **f** GCD curves of NiS/rGO composites at various current densities (0.5–5 A g^{-1}). Adapted with permission from [30], Copyright (2014), Elsevier. **g** LED indicator lighted up by two CNFs-NiS//CNFs Asymmetric Supercapacitor device cells. Adapted with permission from [28], Copyright (2018), Elsevier

depicted in Fig. 2e. The electrode achieved a specific capacity of 235.88 mAh g^{-1} at 1 A g^{-1} and cyclic stability of 87.1% over 2000 cycles. Yang et al. [30] synthesized NiS/rGO composite in which NiS nanorods anchored on rGO via hydrothermal method. Figure 2f displays the GCD curves of NiS/rGO composite at 0.5–5 A g^{-1} current densities. The NiS/rGO electrode achieved 905.30 F g^{-1} specific capacitance at 0.5 A g^{-1} and exhibited cyclic stability of 90.9% over 1000 cycles. Figure 2g shows the LED indicator lighted up by two CNFs-NiS//CNFs Asymmetric Supercapacitor device cells synthesized by Xu et al. [28]. It showed an energy density of 13.32 mWh cm^{-3} and about 89.5% of cyclic stability after 5000 cycles. The NiS based electrode materials are a promising candidate in the field of electrochemical supercapacitor application.

3.2 Nickel Selenide

Zhao et al. [31] developed NiSe@Ni_3Se_2/NF nanostructure by hydrothermal method followed by electrodeposition method. The schematic presentation of synthesis of NiSe@Ni_3Se_2/NF nanostructure is shown in Fig. 3a. The NiSe@Ni_3Se_2/NF nanostructure is made up of NiSe nanowire arrays core and thin Ni_3Se_2 nanosheets shell. Figure 3b shows the NiSe nanowire arrays and such morphology favorable for better electric conductivity and indirectly better theoretical specific capacitance. The prepared NiSe@Ni_3Se_2/NF electrode achieved 1260 F g^{-1} specific capacitance at 10 A g^{-1} and capacity retention of 92.5% after 4000 cycles. The ASC device exhibited an energy density of 45.5 Wh kg^{-1} (at power density 1.600 kW kg^{-1}). Also, it showed capacity retention of 96.1% over 12,000 cycles. Zhao et al. [23] developed binder-less Ni_3Se_2 nanodendrite arrays grown on NF with a one-step solvothermal approach for advanced positive electrodes for supercapacitors. Figure 3c shows the morphology and dendrite-shaped features of Ni_3Se_2 electrodes. Such morphology of Ni_3Se_2 makes it highly electronically conductive, able to provide a more surface area and large number of electrochemical active sites. The as synthesized electrode achieved 1234 F g^{-1} specific capacitance at 1 A g^{-1}. Arul et al. [32] prepared $NiSe_2$/$Ni(OH)_2$ nanocomposites with hydrothermal method followed by ultrasonication method. Figure 3d depicts the FESEM image of hexapod-like $NiSe_2$ microstructure. Such Hexapod-like microstructures are made up of less than ~10 nm nanoparticles.

The prepared electrode exhibited 2212 F g^{-1} specific capacitance at 2 mA cm^{-2} with cyclic stability of 95% for 5000 cycles. Tian et al. [33] prepared NiSe nanorod arrays on a NF current collector with a one-pot hydrothermal method. Figure 3e depicts the GCD curves of NiSe NRA/NF electrode at 5–50 mA cm^{-2} current densities. The NiSe electrode achieved 6.81 F cm^{-2} specific capacitance at 5 mA cm^{-2}. The assembled ASC device (NiSe NRA/NF//RGO) retained 90.09% initial capacitance over 3000 cycles. Wang et al. [34] developed truncated cube-like crystals of $NiSe_2$ via a simple hydrothermal method. Figure 3f presents estimated specific capacitance from the galvanostatic charge-discharge curve versus applied current density of the $NiSe_2$ electrode. The cube-like $NiSe_2$ electrode shows a maximum 1044 F

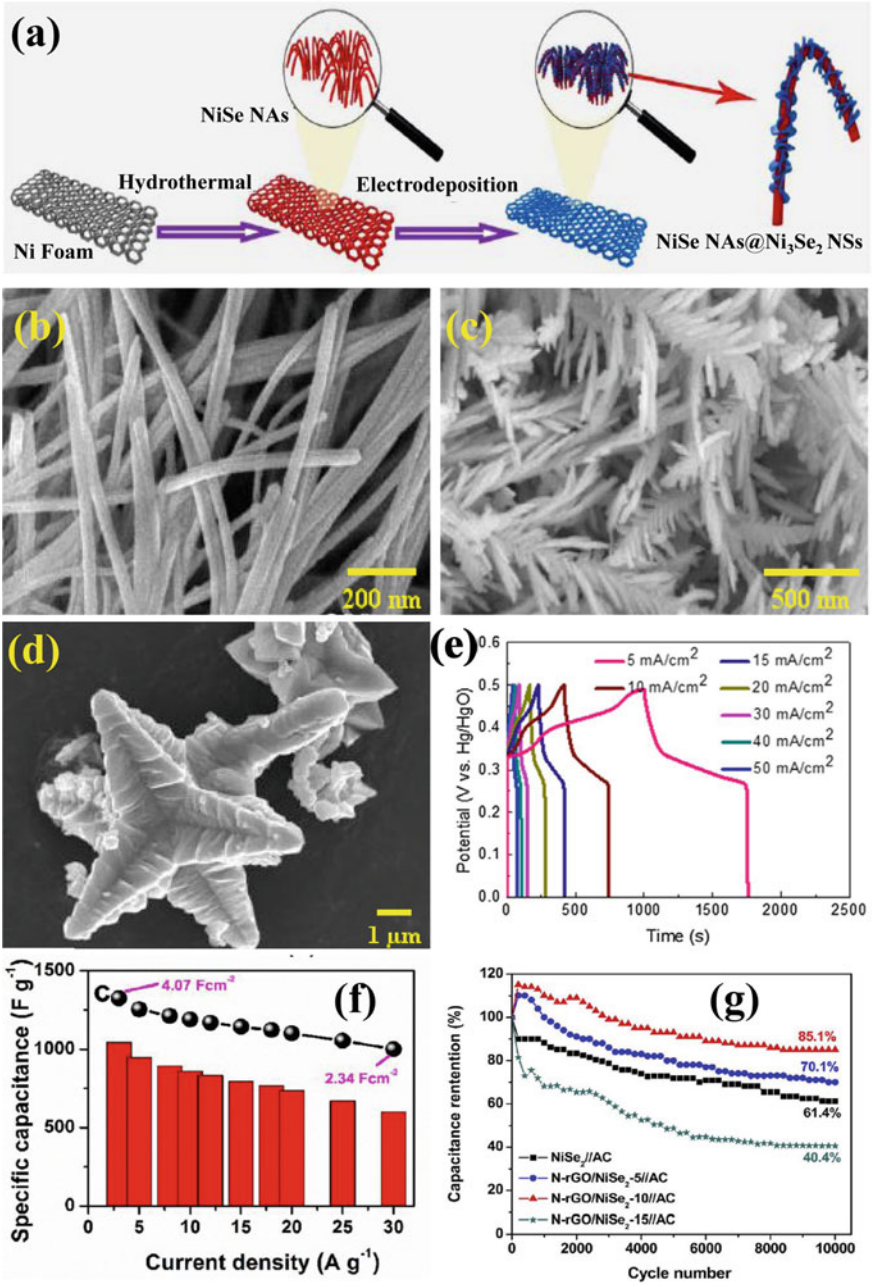
(a)
NiSe NAs
Hydrothermal
Electrodeposition
Ni Foam
NiSe NAs@Ni3Se2 NSs
(b)
200 nm
(c)
500 nm
(d)
1 µm
(e)
5 mA/cm2
10 mA/cm2
15 mA/cm2
20 mA/cm2
30 mA/cm2
40 mA/cm2
50 mA/cm2
Potential (V vs. Hg/HgO)
Time (s)
(f)
4.07 Fcm-2
2.34 Fcm-2
Specific capacitance (F g-1)
Current density (A g-1)
(g)
85.1%
70.1%
61.4%
40.4%
NiSe2//AC
N-rGO/NiSe2-5//AC
N-rGO/NiSe2-10//AC
N-rGO/NiSe2-15//AC
Capacitance rentention (%)
Cycle number

◀**Fig. 3** **a** Schematic presentation of synthesis of NiSe nanowire arrays (NWAs) @ Ni_3Se_2 nanosheets (NSs) composites by hydrothermal method followed by electrodeposition method. Adapted with permission from [31], Copyright (2021), Elsevier. **b** SEM image of NiSe NWAs. Adapted with permission from [31], Copyright (2021), Elsevier. **c** SEM image of Ni_3Se_2 electrode. Adapted with permission from [23], Copyright (2020), Elsevier. **d** FESEM image of $NiSe_2$ electrode. Adapted with permission from [32], Copyright (2019), Elsevier. **e** GCD curves of NiSe NRA/NF electrode at various current densities (5–50 mA cm^{-2}). Adapted with permission from [33], Copyright (2017), Elsevier. **f** Graph of specific capacitance vs current density of $NiSe_2$ electrode. Adapted with permission from [34], Copyright (2017), Elsevier. **g** cyclic stability test of for $NiSe_2$//AC, N-rGO/$NiSe_2$-5//AC, N-rGO/$NiSe_2$-10//AC and N-rGO/$NiSe_2$-15//AC asymmetric supercapacitors at a current density of 5 A g^{-1}. Adapted with permission from [35], Copyright (2019), Elsevier

g^{-1} specific capacitance at 3 A g^{-1}. The prepared $NiSe_2$//AC ASC device shows 87.4% capacity retention over 20,000 cycles. Gu et al. [35] prepared N-rGO/$NiSe_2$ composite with the help of a two-step method. In actual experimental firstly $Ni(OH)_2$ synthesized by simple hydrothermal method and then N-rGO/$NiSe_2$ nanocomposites with different content of N-rGO by solvothermal method. The amount of GO used in the synthesis of composites were 0, 5, 10, and 15 mg. Accordingly, the obtained composites were named $NiSe_2$, N-rGO/$NiSe_2$-5, N-rGO/$NiSe_2$-10, and N-rGO/$NiSe_2$-15 which exhibited higher specific capacitance of 720.8, 1270.4, 2451.4, and 616.0 F g^{-1} at 1 A g^{-1}. Also, they prepared an ASC device with prepared composites and AC. Out of different ASC devices, the N-rGO/$NiSe_2$-10//AC device shows maximum specific capacitance of 113.8 F g^{-1} at a current density of 1 A g^{-1}. Figure 3g shows the cyclic stability test for $NiSe_2$//AC, N-rGO/$NiSe_2$-5//AC, N-rGO/$NiSe_2$-10//AC, and N-rGO/$NiSe_2$-15//AC ASC device at a current density of 5 A g^{-1}. The N-rGO/$NiSe_2$-10//AC ASC device showed better capacity retention of 85.1% after 10,000 cycles. The study reveals that the NiSe based electrodes are promising materials for supercapacitor application.

3.3 Nickel Telluride

Deshagani et al. [36] synthesized selenide dopped nickel telluride (NiTe: Se) flakes by facile hydrothermal method. The experimental procedure of synthesis of NiTe:Se@NF, synthesis of AC from dried coconut shell, and synthesis of poly(N-methyl pyrrole) (PMP) is depicted in Fig. 4a. The SEM study shows the compositional transformation i.e. doping of NiTe with Se produces NiTe:Se, and morphology changes from fiber-like to flakelike morphology. The as-prepared electrode achieved a 634 F g^{-1} specific capacitance at 1 A g^{-1}. The prepared PMP@AC//PMP@NiTe:Se supercapacitor exhibited a capacity of 404 C g^{-1}. Zhou et al. [18] developed NiTe rods on NF by simple hydrothermal method. Figure 4b shows the FESEM image of the NiTe electrode shows a maximum specific capacitance of 804 F g^{-1} (at 1 A g^{-1}). The fabricated ASC device with NiTe as anode and AC as a cathode (NiTe//AC) achieved

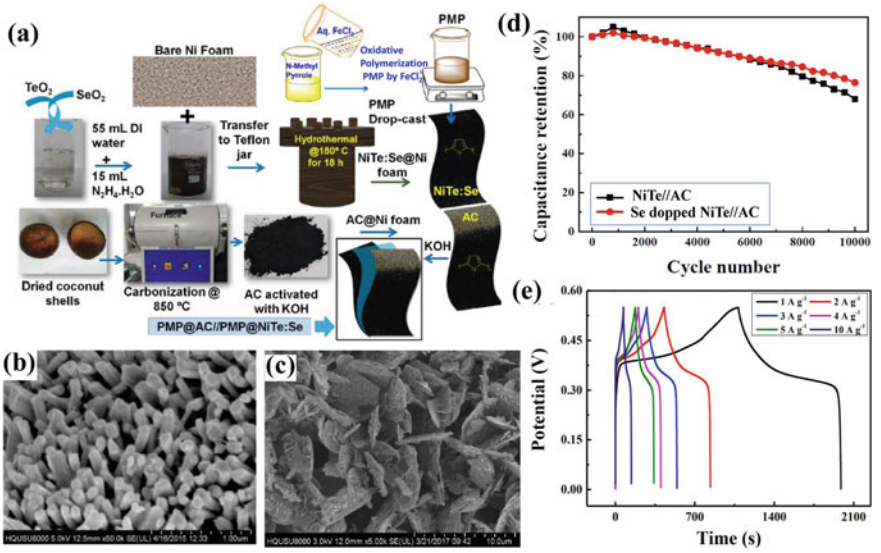

Fig. 4 **a** Schematic diagram of the synthesis of PMP@AC//PMP@ NiTe:Se device. Adapted with permission from [36], Copyright (2020), Elsevier. **b** FESEM images of NiTe rods. Adapted with permission from [18], Copyright (2016), Elsevier. **c** FESEM images of Se doped NiTe with 9:100 doping ratio of Se:Te. Adapted with permission from [37], Copyright (2018), Elsevier. **d** Cycling performances of NiTe and Se doped NiTe electrodes at a current density of 2 A g^{-1}. Adapted with permission from [37], Copyright (2018), Elsevier. **e** GCD curve of NiTe:Co electrode at current densities (1–10 A g^{-1}). Adapted with permission from [24], Copyright (2019), Elsevier

a maximum energy density of 33.6 Wh kg^{-1} and power density of 807.9 W kg^{-1}. It exhibited cyclic stability of about 81% over 3000 cycles. Ye et al. [37] prepared Se doped NiTe electrode materials by using a hydrothermal method on Ni-foam. Figure 4c shows the FESEM image of Se doped NiTe with a 9:100 doping ratio of Se:Te. Such electrode showed 603.6 F g^{-1} specific capacitance at a current density of 1 A g^{-1}. Figure 4d shows the cyclic stability of Se doped NiTe and pristine NiSe electrodes.

The estimated capacitance of the NiTe with Se doped electrode after 1000 cycling is almost constant. The pristine NiTe without Se doping also exhibited better capacity retention of 93.2% over 1000 cycles. The fabricated ASC device achieved a 119.9 F g^{-1} specific capacitance at 1 A g^{-1} and excellent cyclic stability of 76.4% after 10,000 cycles. Ye et al. [24] also synthesized Co-doped NiTe on NF by one-step hydrothermal method. The doping of Co ions in NiTe changes the original microstructure of NiTe as well as improves the electrochemical properties. Figure 4e shows the GCD curve of NiTe: Co electrode at different current densities (1–10 A g^{-1}). The estimated maximum specific capacitance of NiTe: Co electrode is 1445.6 F g^{-1} at 1 A g^{-1}. The as fabricated NiTe: Co//AC device provided an energy density of 36.8 Wh kg^{-1} than the NiTe//AC device (24.4 Wh kg^{-1}).

4 Concluding Remark

This chapter describes a brief overview of NiX (X = S, Se, Te) electrode materials for their electrochemical supercapacitor application. Such electrode materials have been unveiled as cost-effective, promising, and environmentally friendly materials for the fabrication of scalable and flexible supercapacitors. In the beginning, we discussed some characterizations of NiX based electrodes. We have summarized the electrochemical supercapacitor performance of NiX based electrodes and their composites. The approaches towards modifying the physical and chemical parameters of NiX based electrodes for cheap, highly efficient, and renewable energy devices are still in demand. The NiX based electrodes are still far from commercialization even though they show better results. To complete this target, continued and dedicated research efforts should be needed for the improvement of its mechanisms, electrochemical performance, and electrochemical reactions for commercial applications. Despite all the challenges, ongoing research should be more focused to develop highly conductive binder-less NiX based electrodes and their composites.

Table 1 Literature review on nanostructured NiX (X = S, Se, Te) based electrodes

Sr. No	Electrode material	Morphology	KOH Electrolyte	Specific capacitance	Stability	Ref
1	α-NiS	Cabbage-like	6 M	235.88 mAh g^{-1} at 1 A g^{-1}	87.1% after 2000 cycles	[29]
2	NiS	Flower-like	6 M	603.97 F g^{-1} at 1 A g^{-1}	88.57% after 5000 cycle	[16]
3	NiS	Nanowires	3 M	2187.5 F g^{-1} at 3 mV s^{-1}	78.7% after 8000 cycles	[38]
4	β-NiS	Flower-like	6 M	2425.89 F g^{-1} at 1 A g^{-1}	~100% after 5000 cycles	[25]
5	NiS	Nanoparticles	2 M	177.1 mAh g^{-1} at 1 A g^{-1}	88.7% after 5000 cycles	[28]
6	NiS	Forest-like	1 M	342.1 mA h g^{-1} at 4 mA cm^{-2}	89.4% after 3000 cycles	[39]

(continued)

Table 1 (continued)

Sr. No	Electrode material	Morphology	KOH Electrolyte	Specific capacitance	Stability	Ref
7	Ni_3S_2	Flacky	1 M	786.5 C g^{-1} at 10 mA cm^{-2}	88.6% after 1000 cycles	[22]
8	NiS/NiO	Nanoparticles	2 M	1260 F g^{-1} at 0.5 A g^{-1}	–	[40]
9	NiS-MoS_2	Hetero-nanosheet arrays	6 M	271.7 mAh g^{-1} at 2.5 mA cm^{-2}	78% after 3000 cycles	[27]
10	Ni_3S_4–NiS@rGO	Starfish like	2 M	1073 F g^{-1} at 0.5 A g^{-1}	91% after 5000 cycles	[26]
11	NiS/rGO	Porous microstructures	6 M	305 F g^{-1} at 1.1 A g^{-1}	91% after 3000 cycles	[41]
12	Gaphene@NiS	Graphene wrapped nanoprisms	2 M	1000 F g^{-1} at 5 A g^{-1}	71% after 2000 cycles	[42]
13	NiS/rGO	Nanorods anchored on rGO	2 M	905.30 F g^{-1} at 0.5 A g^{-1}	90.9% after 1000 cycles	[30]
14	NiS/rGO	Nanorods anchored on graphene	2 M	744 C g^{-1} at 1 A g^{-1}	89% after 20,000 cycles	[43]
15	Ni_xS_y/rGO	Nanoflakes	2 M	2074 F g^{-1} at 1 A g^{-1}	80% after 5000 cycles	[44]
16	Ni_3Se_2	Nanodendrite arrays	2 M	1234 F g^{-1} at 1 A g^{-1}	Good cyclic stability	[23]
17	Ni_3Se_2	Nanowires	2 M	2.6 C cm^{-2} at 5 mA cm^{-2}	93.1% after 2000 cycles	[45]
18	Ni_3Se_2	Nanosheets	3 M	854 F g^{-1} at 1 A g^{-1}	87.23% after 2000 cycles	[46]

(continued)

Table 1 (continued)

Sr. No	Electrode material	Morphology	KOH Electrolyte	Specific capacitance	Stability	Ref
19	$Ni_{0.85}Se$	Honeycomb like nanosheets	3 M	3105 F g^{-1} at 1 A g^{-1}	90.1% after 5000 cycles	[47]
20	$NiSe_2$	Spheres	2 M	1144.1 F g^{-1} at 0.5 A g^{-1}	Good cyclic stability	[48]
21	$NiSe_2$	Hollow spheres	2 M	341 F g^{-1} at 1 A g^{-1}	Good cyclic stability	[49]
22	$NiSe_2$	2D nanosheets	1 M	466 F g^{-1} at 5 mV s^{-1}	81.3% after 1000 cycles	[50]
23	NiSe	Nanorod arrays	6 M	6.81 F cm^{-2} at 5 mA cm^{-2}	78.9% after 2000 cycles	[33]
24	$NiSe_2$	Truncated cube-like	4 M	1044 F g^{-1} at 3 A g^{-1}	67% after 2000 cycles	[34]
25	$NiSe_2$	Pyramid-like	3 M	240.83 mAh g^{-1} at 1 A g^{-1}	52.7% after 1000 cycles	[51]
26	NiSe-$Ni_{0.85}Se$	Irregular nanoparticle	2 M	669 C g^{-1} at 1 A g^{-1}	–	[52]
27	NiSe@Ni_3Se_2	Nanosheet nanowire arrays	3 M	1260 F g^{-1} at 10 A g^{-1}	92.5% after 4000 cycles	[31]
28	$NiSe_2$/$Ni(OH)_2$	Hexapod-like	3 M	2212 F g^{-1} at 2 mA cm^{-2}	95% after 5000 cycles	[32]
29	NiSe	Microspheres	2 M	492 F g^{-1} at 0.5 A g^{-1}	84.6% after 200 cycles	[53]
30	N-rGO/$NiSe_2$	GO decorated with nanoparticle	3 M	2451.4 F g^{-1} at 1 A g^{-1}	–	[35]
31	$Ni_{0.85}Se$@C/rGO	Nanosheets on the surface of rGO	2 M	1160 F g^{-1} at 1 A g^{-1}	88.8% after 1000 cycles	[54]

(continued)

Table 1 (continued)

Sr. No	Electrode material	Morphology	KOH Electrolyte	Specific capacitance	Stability	Ref
32	$NiSe_2$/rGO	Nanoparticles supported on GO	2 M	137.7 mAh g^{-1} at 1 A g^{-1}	82% after 2500 cycles)	[55]
33	NiTe	Rod like	3 M	804 F g^{-1} at 1 A g^{-1}	91.3% after 1000 cycles	[18]
34	NiTe	Fiber-like	6 M	634 F g^{-1} at 1 A g^{-1}	–	[36]
35	NiTe: Se	Flake-like	6 M	943 F g^{-1} at 1 A g^{-1}	–	[36]
36	NiTe	Nanorods	3.5 M	618 F g^{-1} at 1 A g^{-1}	75% after 5000 cycles	[56]
37	NiTe: Co	Nanoparticles	3 M	1645.6 F g^{-1} at 1 A g^{-1}	90% after 1000 cycles	[24]
38	NiTe	Flake shaped	3 M	872.7 F g^{-1} 1 A g^{-1}	85% after 1000 cycles	[24]
39	Se-doped NiTe	Flake-like	3 M	998.2 F g^{-1} at 1 A g^{-1}	Good cyclic stability over 1000 cycles	[37]
40	NiTe	–	3 M	603.6 F g^{-1} at 1 A g^{-1}	93.2% after 1000 cycles	[37]

Acknowledgements Dr. G. M. Lohar is thankful to DST-SERB, Government of India, for providing funds under the ECRA scheme File No: ECR/2017/002099.

References

1. U.M. Patil, V. V. Patil, A.S. Patil, S.J. Marje, J.L. Gunjakar, C.D. Lokhande, Nanoporous Transition metal oxide-based electrodes for supercapacitor application. Chem. Depos. Nanocrystalline Met. Oxide Thin Film. 623–672 (2021)

2. J. Theerthagiri, A.P. Murthy, S.J. Lee, K. Karuppasamy, S.R. Arumugam, Y. Yu, M.M. Hanafiah, H.S. Kim, V. Mittal, M.Y. Choi, Recent progress on synthetic strategies and applications of transition metal phosphides in energy storage and conversion. Ceram. Int. **47**, 4404–4425 (2021)
3. H. Yuan, L. Kong, T. Li, Q. Zhang, A review of transition metal chalcogenide/graphene nanocomposites for energy storage and conversion. Chinese Chem. Lett. **28**, 2180–2194 (2017)
4. O.C. Pore, A.V. Fulari, R.V. Shejwal, V.J. Fulari, G.M. Lohar, Review on recent progress in hydrothermally synthesized MCo2O4/rGO composite for energy storage devices, Chem. Eng. J. **426**, 131544 (2021)
5. M. Sajjad, F. Cheng, W. Lu, Research progress in transition metal chalcogenide based anodes for K-ion hybrid capacitor applications: a mini-review. RSC Adv. **11**, 25450–25460 (2021)
6. C. Xia, Q. Jiang, C. Zhao, P.M. Beaujuge, H.N. Alshareef, Asymmetric supercapacitors with metal-like ternary selenides and porous graphene electrodes. Nano Energy **24**, 78–86 (2016)
7. J. Theerthagiri, K. Karuppasamy, G. Durai, A. ul H.S. Rana, P. Arunachalam, K. Sangeetha, P. Kuppusami, H.S. Kim, Recent advances in metal chalcogenides (MX; X = S, Se) nanostructures for electrochemical supercapacitor applications: a brief review. Nanomaterials **8**, 256 (2018)
8. G.A. Muller, J.B. Cook, H.-S. Kim, S.H. Tolbert, B. Dunn, High performance pseudocapacitor based on 2D layered metal chalcogenide nanocrystals. Nano Lett. **15**, 1911–1917 (2015)
9. H. Chauhan, S. Deka, Supercapacitors based on two-dimensional transition metal dichalcogenides and their hybrids, Fundam. Supercapacitor Appl. 2D Mater. 159–191 (2021)
10. M.J. Crane, M.B. Lim, X. Zhou, P.J. Pauzauskie, Rapid synthesis of transition metal dichalcogenide–carbon aerogel composites for supercapacitor electrodes. Microsystems Nanoeng. **3**, 17032 (2017)
11. Y. Wang, Y. Zhao, X. Ding, L. Qiao, Recent advances in the electrochemistry of layered post-transition metal chalcogenide nanomaterials for hydrogen evolution reaction. J. Energy Chem. **60**, 451–479 (2021)
12. N.M. Santhosh, K.K. Upadhyay, P. Stražar, G. Filipič, J. Zavašnik, A.M. de Ferro, R.P. Silva, E. Tatarova, M. de F. Montemor, U. Cvelbar, Advanced carbon–nickel sulfide hybrid nanostructures: extending the limits of battery-type electrodes for redox-based supercapacitor applications. ACS Appl. Mater. Interfaces. **13**, 20559–20572 (2021)
13. M. Manikandan, K. Subramani, S. Dhanuskodi, M. Sathish, One-pot hydrothermal synthesis of nickel cobalt telluride nanorods for hybrid energy storage systems. Energy Fuels **35**, 12527–12537 (2021)
14. O. Maurya, S. Khaladkar, M.R. Horn, B. Sinha, R. Deshmukh, H. Wang, T. Kim, D.P. Dubal, A. Kalekar, Emergence of Ni-based chalcogenides (S and Se) for clean energy conversion and storage. Small **17**, 2100361 (2021)
15. R.N.A.R. Seman, M.A. Azam, M.H. Ani, Graphene/transition metal dichalcogenides hybrid supercapacitor electrode: status, challenges, and perspectives. Nanotechnology **29**, 502001 (2018)
16. N. Parveen, S.A. Ansari, S.G. Ansari, H. Fouad, N.M. Abd El-Salam, M.H. Cho, Solid-state symmetrical supercapacitor based on hierarchical flower-like nickel sulfide with shape-controlled morphological evolution. Electrochim. Acta. **268**, 82–93 (2018)
17. S. Wu, Q. Hu, L. Wu, J. Li, H. Peng, Q. Yang, One-step solvothermal synthesis of nickel selenide nanoparticles as the electrode for high-performance supercapacitors. J. Alloys Compd. **784**, 347–353 (2019)
18. P. Zhou, L. Fan, J. Wu, C. Gong, J. Zhang, Y. Tu, Facile hydrothermal synthesis of NiTe and its application as positive electrode material for asymmetric supercapacitor. J. Alloys Compd. **685**, 384–390 (2016)
19. R. Karthikeyan, D. Thangaraju, N. Prakash, Y. Hayakawa, Single-step synthesis and catalytic activity of structure-controlled nickel sulfide nanoparticles. CrystEngComm **17**, 5431–5439 (2015)
20. X. Li, J. Shen, N. Li, M. Ye, Template-free solvothermal synthesis of NiS2 microspheres on graphene sheets for high-performance supercapacitors. Mater. Lett. **139**, 81–85 (2015)
21. D. Song, H. Wang, X. Wang, B. Yu, Y. Chen, NiSe2 nanoparticles embedded in carbon nanowires as highly efficient and stable electrocatalyst for hydrogen evolution reaction. Electrochim. Acta. **254**, 230–237 (2017)

22. D. Kim, P.K. Kannan, S. Mateti, C.-H. Chung, Indirect nanoconstruction morphology of Ni3S2 electrodes renovates the performance for electrochemical energy storage. ACS Appl. Energy Mater. **1**, 6945–6952 (2018)
23. L. Zhao, P. Zhang, Y. Zhang, Z. Zhang, L. Yang, Z.G. Chen, Facile synthesis of hierarchical Ni3Se2 nanodendrite arrays for supercapacitors. J. Mater. Sci. Technol. **54**, 69–76 (2020)
24. B. Ye, M. Huang, L. Fan, J. Lin, J. Wu, Co ions doped NiTe electrode material for asymmetric supercapacitor application. J. Alloys Compd. **776**, 993–1001 (2019)
25. Y. Zhang, J. Zhang, D. Ding, Y. Gao, Controllable synthesis of three-dimensional β-NiS nanostructured assembly for hybrid-type asymmetric supercapacitors. Nanomater **10**, 487 (2020)
26. S. Azizi Darsara, M. Seifi, M.B. Askari, M. Osquian, Hierarchical 3D starfish-like Ni3S4–NiS on reduced graphene oxide for high-performance supercapacitors. Ceram. Int. **47**, 20992–20998 (2021)
27. S. Guan, X. Fu, Z. Lao, C. Jin, Z. Peng, NiS-MoS2 hetero-nanosheet arrays on carbon cloth for high-performance flexible hybrid energy storage devices. ACS Sustain. Chem. Eng. **7**, 11672–11681 (2019)
28. J. Xu, L. Zhang, G. Xu, Z. Sun, C. Zhang, X. Ma, C. Qi, L. Zhang, D. Jia, Facile synthesis of NiS anchored carbon nanofibers for high-performance supercapacitors. Appl. Surf. Sci. **434**, 112–119 (2018)
29. Y. Tan, W.D. Xue, Y. Zhang, D.X. He, W.J. Wang, R. Zhao, Solvothermal synthesis of hierarchical α-NiS particles as battery-type electrode materials for hybrid supercapacitors. J. Alloys Compd. **806**, 1068–1076 (2019)
30. J. Yang, X. Duan, W. Guo, D. Li, H. Zhang, W. Zheng, Electrochemical performances investigation of NiS/rGO composite as electrode material for supercapacitors. Nano Energy **5**, 74–81 (2014)
31. J. Zhao, L. Yang, H. Li, T. Huang, H. Cheng, A. Meng, Y. Lin, P. Wu, X. Yuan, Z. Li, Ni3Se2 nanosheets in-situ grown on 3D NiSe nanowire arrays with enhanced electrochemical performances for supercapacitor and efficient oxygen evolution. Mater. Charact. **172**, 110819 (2021)
32. N.S. Arul, J.I. Han, Enhanced pseudocapacitance of NiSe2/Ni(OH)2 nanocomposites for supercapacitor electrode. Mater. Lett. **234**, 87–91 (2019)
33. Y. Tian, Y. Ruan, J. Zhang, Z. Yang, J. Jiang, C. Wang, Controllable growth of NiSe nanorod arrays via one-pot hydrothermal method for high areal-capacitance supercapacitors. Electrochim. Acta. **250**, 327–334 (2017)
34. S. Wang, W. Li, L. Xin, M. Wu, Y. Long, H. Huang, X. Lou, Facile synthesis of truncated cube-like NiSe2 single crystals for high-performance asymmetric supercapacitors. Chem. Eng. J. **330**, 1334–1341 (2017)
35. Y. Gu, L.Q. Fan, J.L. Huang, C.L. Geng, J.M. Lin, M.L. Huang, Y.F. Huang, J.H. Wu, N-doped reduced graphene oxide decorated NiSe2 nanoparticles for high-performance asymmetric supercapacitors. J. Power Sources **425**, 60–68 (2019)
36. S. Deshagani, P. Ghosal, M. Deepa, Altered crystal structure of nickel telluride by selenide doping and a poly(N-methylpyrrole) coating amplify supercapacitor performance. Electrochim. Acta **345**, 136200 (2020)
37. B. Ye, M. Huang, S. Jiang, L. Fan, J. Lin, J. Wu, In-situ growth of Se-doped NiTe on nickel foam as positive electrode material for high-performance asymmetric supercapacitor. Mater. Chem. Phys. **211**, 389–398 (2018)
38. Y. Xu, W. Du, L. Du, W. Zhu, W. Guo, J. Chang, B. Zhang, D. Deng, Monocrystalline NiS nanowire arrays supported by Ni foam as binder-free electrodes with outstanding performances, RSC Adv. **7**, 22553–22557 (2017)
39. G.S.R. Raju, E. Pavitra, G. Nagaraju, S.C. Sekhar, S.M. Ghoreishian, C.H. Kwak, J.S. Yu, Y.S. Huh, Y.-K. Han, Rational design of forest-like nickel sulfide hierarchical architectures with ultrahigh areal capacity as a binder-free cathode material for hybrid supercapacitors. J. Mater. Chem. A. **6**, 13178–13190 (2018)

40. H. Wang, J. Wang, M. Liang, Z. He, K. Li, W. Song, S. Tian, W. Duan, Y. Zhao, Z. Miao, Novel dealloying-fabricated NiS/NiO nanoparticles with superior cycling stability for supercapacitors. ACS Omega **6**, 17999–18007 (2021)
41. N.A. Marand, S.M. Masoudpanah, S. Alamolhoda, M.S. Bafghi, Solution combustion synthesis of nickel sulfide/reduced graphene oxide composite powders as electrode materials for high-performance supercapacitors, J. Energy Storage **39**, 102637 (2021)
42. A.A. AbdelHamid, X. Yang, J. Yang, X. Chen, J.Y. Ying, Graphene-wrapped nickel sulfide nanoprisms with improved performance for Li-ion battery anodes and supercapacitors. Nano Energy **26**, 425–437 (2016)
43. C. Qu, L. Zhang, W. Meng, Z. Liang, B. Zhu, D. Dang, S. Dai, B. Zhao, H. Tabassum, S. Gao, H. Zhang, W. Guo, R. Zhao, X. Huang, M. Liu, R. Zou, MOF-derived α-NiS nanorods on graphene as an electrode for high-energy-density supercapacitors. J. Mater. Chem. A. **6**, 4003–4012 (2018)
44. S. Dai, B. Zhao, C. Qu, D. Chen, D. Dang, B. Song, B.M. deGlee, J. Fu, C. Hu, C.P. Wong, M. Liu, Controlled synthesis of three-phase NixSy/rGO nanoflake electrodes for hybrid supercapacitors with high energy and power density. Nano Energy **33**, 522–531 (2017)
45. W. Li, T. Chen, A. Li, P. Shi, M. Wu, T. Li, H. Yue, Y. Chen, B. Huang, X. Lou, High energy density hybrid supercapacitors derived from novel Ni3Se2 nanowires in situ constructed on porous nickel foam. Inorg. Chem. Front. **8**, 1093–1101 (2021)
46. S. Jiang, J. Wu, B. Ye, Y. Fan, J. Ge, Q. Guo, M. Huang, Growth of Ni3Se2 nanosheets on Ni foam for asymmetric supercapacitors. J. Mater. Sci. Mater. Electron. **29**, 4649–4657 (2018)
47. L. Du, W. Du, H. Ren, N. Wang, Z. Yao, X. Shi, B. Zhang, J. Zai, X. Qian, Honeycomb-like metallic nickel selenide nanosheet arrays as binder-free electrodes for high-performance hybrid asymmetric supercapacitors. J. Mater. Chem. A. **5**, 22527–22535 (2017)
48. J. Yang, Z. Sun, J. Wang, J. Zhang, Y. Qin, J. You, L. Xu, Hierarchical NiSe2 spheres composed of tiny nanoparticles for high performance asymmetric supercapacitors. CrystEngComm **21**, 994–1000 (2019)
49. M. Lu, X.-P. Yuan, X.-H. Guan, G.-S. Wang, Synthesis of nickel chalcogenide hollow spheres using an L-cysteine-assisted hydrothermal process for efficient supercapacitor electrodes. J. Mater. Chem. A. **5**, 3621–3627 (2017)
50. A. Chang, C. Zhang, Y. Yu, Y. Yu, B. Zhang, Plasma-assisted synthesis of NiSe2 ultrathin porous nanosheets with selenium vacancies for supercapacitor. ACS Appl. Mater. Interfaces. **10**, 41861–41865 (2018)
51. L. Meng, Y. Wu, T. Zhang, H. Tang, Y. Tian, Y. Yuan, Q. Zhang, Y. Zeng, J. Lu, Highly conductive NiSe2 nanostructures for all-solid-state battery–supercapacitor hybrid devices. J. Mater. Sci. **54**, 571–581 (2019)
52. Y. Bai, W. Shen, K. Song, S. Zhang, Y. Wang, T. Xu, J. Xu, S. Dai, X. Wang, Controlled synthesis of NiSe-Ni0.85Se nanocomposites for high-performance hybrid supercapacitors. J. Electroanal. Chem. **880**, 114795 (2021)
53. K. Guo, F. Yang, S. Cui, W. Chen, L. Mi, Controlled synthesis of 3D hierarchical NiSe microspheres for high-performance supercapacitor design. RSC Adv. **6**, 46523–46530 (2016)
54. Z. Sun, F. Liu, J. Wang, Y. Hu, Y. Fan, S. Yan, J. Yang, L. Xu, Tiny Ni0.85Se nanosheets modified by amorphous carbon and rGO with enhanced electrochemical performance toward hybrid supercapacitors. J. Energy Storage **29**, 101348 (2020)
55. S. Wu, T. Cui, Q. Hu, F. Yin, Q. Feng, S. Zhou, Q. Su, L. Wu, Q. Yang, Mixing solvothermal synthesis nickel selenide on the surface of graphene for high-efficiency asymmetric supercapacitors. Synth. Met. **268**, 116490 (2020)
56. M. Manikandan, K. Subramani, M. Sathish, S. Dhanuskodi, NiTe nanorods as electrode material for high performance supercapacitor applications. ChemistrySelect **3**, 9034–9040 (2018)